THE ASTROPHYSICAL JOURNAL, 352:44–54, 1990 March 20

LONG-SLIT SPECTROSCOPY OF 3C 31, 3C 75, 3C 465, NGC 1265, AND CYGNUS A

FRAZER N. OWEN[1]
National Radio Astronomy Observatory[2]
CHRISTOPHER P. O'DEA[1]
National Radio Astronomy Observatory
AND
WILLIAM C. KEEL[3]
National Optical Astronomy Observatories;[4] and University of Alabama
Received 1989 July 3; accepted 1989 September 19

ABSTRACT

We present results of long slit optical spectroscopy of five radio galaxies (3C 31, 3C 75, 3C 83.1B [NGC 1265], 3C 405 [Cygnus A], and 3C 465). We oriented the slit at various different positions with respect to the radio sources in order to look for emission from plasma in the radio jets and lobes, hypothetical dense clouds at bends in the jets, and emission from the general surrounding medium.

In most cases no extra-nuclear emission was detected. This allows us to set temperature and density limits for gas in the various volumes studied assuming equilibrium with the pressures implied by *Einstein* X-ray observations. These limits were obtained mainly from the Hα, Fe X (λ6374), and Fe XIV (λ5303) lines. These results rule out or set constraints on a number of models for the radio sources.

We rule out models involving cool deflecting clouds for bending 3C 465 and 3C 75, except with a very unlikely combination of parameters. We also find that our data is inconsistent with heavy jet models for 3C 31. The temperature in the interstellar medium of NGC 1265 is found to exceed 3×10^6 K and that the interstellar magnetic field must exceed 0.08 μG. We also find that the large rotation measures seen in Cygnus A are probably produced in a foreground screen of *hot* gas rather than in a cool boundary layer between the radio source and the intercluster medium.

In 3C 31, in addition to obtaining limits far from the nucleus, we detected extended emission apparently associated with a rotating disk of gas associated with a dust lane originally reported by Butcher, van Breugel, and Miley.

Subject headings: galaxies: jets — galaxies: structure — radio sources: galaxies

I. INTRODUCTION

Our knowledge of the radio structures associated with radio jets and lobes continues to improve. Observations made at Westerbork and the VLA have revealed complex, twisted radio structures and provided spectral index and Faraday rotation maps. Central to much of the theoretical interpretation of these data is the density and temperature in and around the radio sources. Most of this gas appears to be hot, 10^7 to 10^8 K, as revealed by *Einstein* X-ray observations of the associated galaxies or clusters of galaxies. However, cooler, denser gas has been found associated with some radio systems (e.g., Heckman, van Breugel, and Miley 1984; Baum *et al.* 1988) and could well be responsible for some of the phenomena seen on the radio maps. In other cases cool gas is not expected from the models but remains a logical possibility and needs to be ruled out (or detected) in order to limit parameter space.

Examples of outstanding problems which would be affected by the existence of cool gas associated with radio sources are:

1. In radio galaxies with luminosities[5] $< 10^{25}$ W Hz^{-1} sr^{-1} at 1400 MHz the mass flux in radio jets is thought to be dominated by thermal gas. The jets are also believed to be lighter (less dense) than the surrounding medium. However, jets of cool, dense gas remain a possibility.

2. These same jets in low-luminosity sources should be entraining the external medium through a turbulent boundary layer. This gas might well be compressed and then cool in the process. Direct observations of this process would constrain models for turbulent entraining jets (Bicknell 1986; De Young 1986).

3. The origin of the bent structures seen in the Wide-Angle Tail (WAT) radio morphology associated with dominant cluster members is still not well understood. Eilek *et al.* 1984 have suggested that the jets could be bent by collisions with cool, dense clouds (10^4 K, 10 cm^{-3}) in the intracluster medium (ICM). The predicted Hα emission should be detectable.

4. Very large rotation measure gradients (6000 rad m^{-2}) across the radio structure of Cygnus A have recently been reported (Dreher, Carilli, and Perley 1987). Existence of cool, dense gas surrounding the radio lobes would make the large gradients easier to understand.

In order to study these problems, we report long-slit spectro-

[1] Visiting Astronomer at NOAO.
[2] Operated by Associated Universities, Inc., under contract with the National Science Foundation.
[3] Now at the University of Alabama.
[4] Operated by the Association of Universities for Research in Astronomy, Inc., under contract with the National Science Foundation.

[5] $H_0 = 75$ km s^{-1} Mpc^{-1} and $q_0 = 0.0$.

TABLE 1

JOURNAL OF OBSERVATIONS

Object	P.A.°	Exposure (min)	Airmass	Date	Remarks
3C 465 S	145	2 × 30 + 15	1.15	1984 Aug 22–23	...
3C 465 S	136	30	1.03	1984 Aug 22–23	...
NGC 1265	95	3 × 10	1.47	1984 Aug 22–23	...
NGC 1265	95	10 + 14	1.29	1984 Aug 22–23	2".5 N of nucleus; clouds
3C 31	160	30	1.16	1984 Aug 23–24	Along jet
NGC 1265	178	30	1.38	1984 Aug 23–24	6"W of nucleus
3C 75 S	145	2 × 30 + 15	1.17	1984 Aug 23–24	Along jets
Cygnus A	106	2 × 15 + 30	1.04	1984 Aug 23–24	Along jet

scopic observations of five radio galaxies with the Cryo Camera on the 4 m Mayall telescope at Kitt Peak National Observatory.

II. SPECTROSCOPY AND DATA ANALYSIS

a) Observations

Previous limits on the emission from 10^4 to 10^6 K gas in radio galaxies have generally come from imaging with narrow band Hα or [O III] filters. This technique has the advantage of imaging the entire galaxy but the disadvantage of lower sensitivity due to the relatively poor match between the filter width and the actual emission line width. Also, only one emission line is obtained at a time. With the long slit on the cryo camera we can gain the optimum resolution for detection of the lines and we can detect or put limits on many lines at once. However, we must pick our one-dimensional cut across the face of the galaxy carefully in order to intersect the most physically interesting parts of the system. We have obtained spectra of five radio galaxies, observing a variety of positions to encompass the bend areas, inner jets, lobes, and in NGC 1265 regions up- and downstream along the direction suggested by the outer tail structure. The spectra were obtained during the nights 1984 August 22–24 (UT) with the Cryogenic Camera at the Mayall telescope. This device is a high-efficiency grism spectrometer incorporating a TI 512 × 800 CCD in an evacuated $f/1$ Schmidt camera as the detector. A grism with 600 lines mm^{-1} gave a wavelength range of 4500–8000 Å, at ~4 Å per pixel; the resolution (FWHM) is 15–20 Å depending on the location in the spectrum. The dominant contribution to the instrumental linewidth near the center of the spectrum is the projected slit width, ~12 Å for our slit opening of 2".5; elsewhere, defocussing due to the CCD's departures from flatness is significant, and dominates longward of ~7000 Å. None of the emission features sought occurs redward of 6900 Å in any of our objects, so that this effect is not serious for our purposes.

A journal of observations is given in Table 1. Some observations were obtained through clouds; these are so noted, and their calibration is described below. Our slit positions are shown superimposed on the VLA maps of 3C 31, 3C 75, 3C 83.1B (NGC 1265), 3C 405 (Cygnus A), and 3C 465 in Figures 1–5.

The raw spectra were reduced to arrays of flux (F_λ) versus wavelength and spatial position using the RV routines of the KPNO IPPS. Pixel-to-pixel sensitivity variations were removed through division by a flattened continuum-lamp frame obtained at the beginning of each night; these frames had enough counts per pixel to avoid contributing significantly to the pixel-to-pixel noise level. Each row (along the spectrum) was put on a common linear wavelength scale through mea-

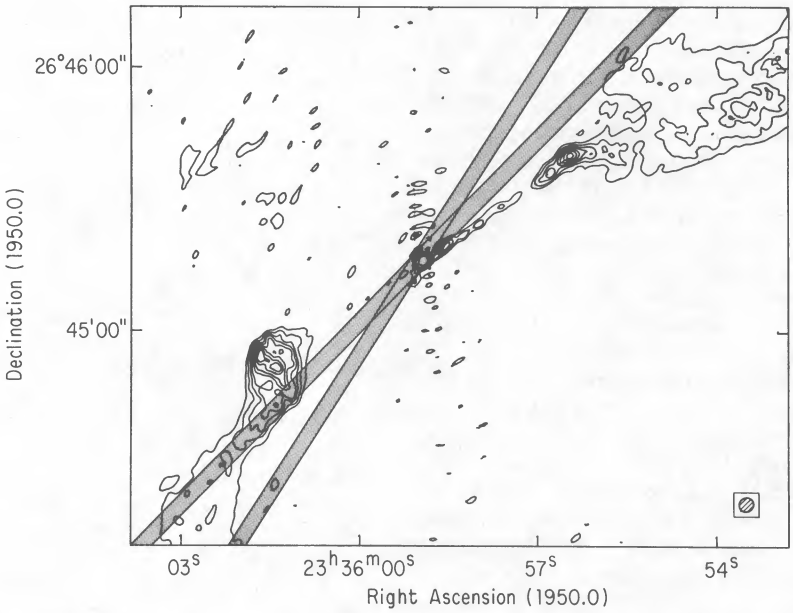

FIG. 1.—Contour plot of the radio source 3C 465 showing the positions of the spectroscope slits (width 2".5 and width 5'). Contour plot is originally from Eilek *et al.* (1984).

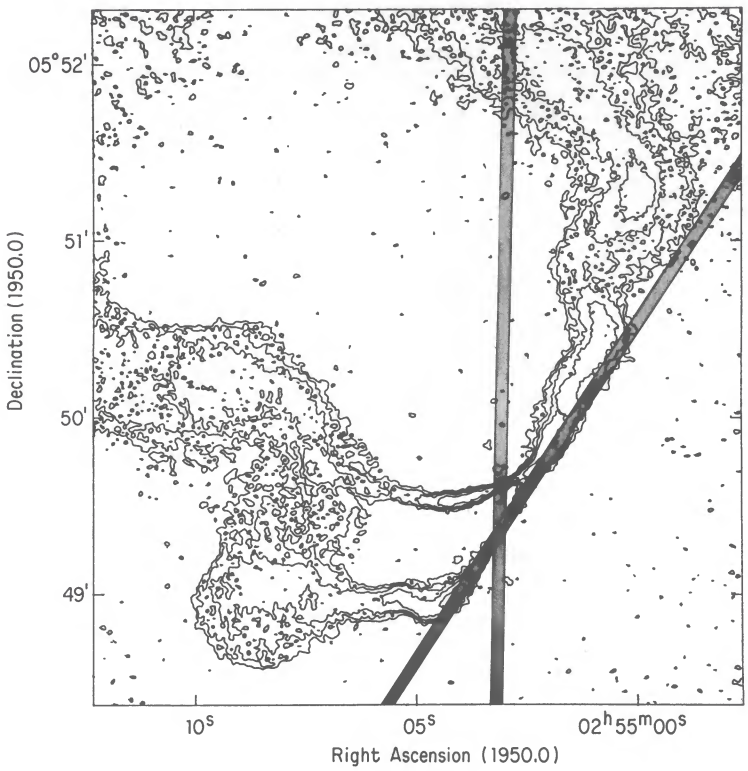

FIG. 2.—Contour plot of the radio source 3C 75 showing the positions of the spectroscope slits (width 2".5 and width 5'). Contour plot is originally from Owen *et al.* 1985.

surement of a He-Ne-Ar comparison lamp made immediately before or after each galaxy observation; the resulting wavelength scale is generally good to ~ 0.5 Å (~ 50 km s^{-1}). Slight misalignment of the slit and grism grooves and small distortions in the optics giving rise to shifts in the object position with wavelength, were removed using measures of standard-star spectra.

A response curve (flux per count per unit time) was generated using observations of the standard stars Kopff 27, Feige 25, and Feige 110 (one or two per night) and a standard extinction curve. Clouds are generally gray enough that this procedure yields accurate relative flux levels within each spectrum; differential atmospheric dispersion is not likely to have serious effects at the airmasses of our observations (Table 1). Experience indicates that the internal accuracy of the flux distributions derived in this way is 5% or better. As a check on our absolute flux scales, and to determine the necessary correction factors for objects observed through clouds, we have used surface photometry in the R band from the KPNO no. 1 0.9 m telescope and an RCA CCD (Owen and White, in 1990). The surface brightness a few arcseconds from the nucleus along our slit positions was used to set the absolute flux scale for our analysis; Hα is near enough to the effective wavelength of the R band, and elliptical galaxy continua are flat enough across the band, that an excellent calibration of the continuum intensity at Hα is possible in this way. Points a few arcseconds from each nucleus were chosen for the normalization to avoid problems which are due to different seeing and point-spread function (PSF) between the imaging and the spectroscopic observations. (Note that portions of the data for NGC 1265 are compromised by the bright star $\sim 2''$ SE of the nucleus.)

b) Imaging Processing and Emission-line Limits

Because of the wide background intensity range over which we have sought emission lines and the large dynamic range of these data (several hundred), there are several distinct regimes in which our sensitivity limits must be defined.

In the outermost regions of the galaxies, where most of the jet bends are found, the starlight intensity is negligible in comparison with the night sky brightness. In this case, the noise sources are the Poisson statistics of the night-sky light at the relevant wavelength combined with the CCDs readout noise of ~ 9 electrons rms per exposure. Readout noise becomes less important for long exposures. The sky level was ~ 65 analog-digital units (ADUs) = 200 electrons (detected photons) per 10 minutes of exposure near 6600 Å, so that readout noise is important but not dominant in most of our individual exposures. The expected rms noise in counts pixel^{-1} for the sum of N exposures is then

$$\sigma_0 = (n_s + N^{1/2} n_r^2)^{1/2} , \quad (1)$$

where n_s is the total number of detected photons per pixel from the sky and n_r (=9) is the readout noise per exposure. To obtain a realistic limit on emission-line flux in a specified area, we must sum over a number of spectral channels representing the instrumental profile plus a (small) additional broadening due to a plausible internal velocity dispersion of the emitting clouds, and across a spatial region (along the slit) as least as large as the PSF (3–4 pixels = 2.5–3".4) and in some cases larger, if suggested by the radio source geometry. The noise (in total detected counts) is now

$$\sigma_1 = \sigma_0 (IJ)^{-1/2} , \quad (2)$$

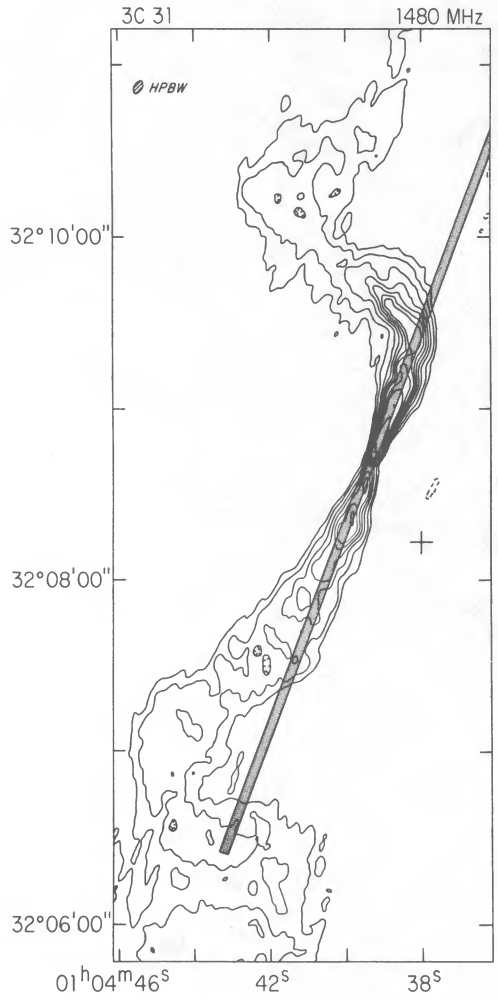

FIG. 3.—Contour plot of the radio source 3C 31 showing the positions of the spectroscope slits (width 2".5 and width 5'). Contour plot is originally from Fomalont *et al.* 1980.

where I and J are the numbers of pixels summed spectrally and spatially. This expression could be confirmed directly by examining the residual counts after sky subtraction in the "blank-sky" regions of our spectra.

Somewhat closer to the galaxy core, the starlight continuum adds an additional background, increasing the noise for emission line studies. A more general formulation including the number of counts per pixel of galaxy light, n_g, at the exact location under consideration is appropriate here:

$$\sigma_2 = (\sum n_g + \sigma_1^2)^{1/2} , \quad (3)$$

where the summation is over the pixels in the spectral and spatial range described by I and J. Near the nucleus, $n_g^{1/2}$ becomes the dominant source of Poisson noise.

Very close to the nucleus, as in examination of the inner jet regions, a more fundamental limitation is reached. Because plausible emission-line widths are of the same order as the central projected stellar velocity dispersions (both barely resolved in our data), weak emission at Hα will appear only as a filling-in of the stellar absorption line. Its detection then depends on how accurately the real Hα strength of the underlying stellar population is known. The Hα equivalent width W_λ(Hα) is ~1.8 Å in elliptical galaxies, with a range of ~10% about this value (Pritchet 1977; Keel 1983). Thus, if no further information is available, the emission could only be detected above a threshold equivalent width of 0.2–0.3 Å, as a decrease in the depth of the absorption line. Since Hα depth gradients across ellipticals are small, a slightly stronger result may be obtained by looking for changes in Hα depth across a galaxy, for example by the flattening procedure described below. This gives an improvement ~30%, perhaps reaching a limit of 0.15 Å in the best cases. Translated to a fraction of the continuum intensity, for a 5 pixel (20 Å) strip of arbitrary spatial extent, W_λ(Hα) = 0.15 Å corresponds to 7.5×10^{-3} of the counts detected. This limit is reached at 2×10^4 detected counts per 20 Å bin, above which emission will be detected only if it exceeds

$$\sigma_3 = 7.5 \times 10^{-3} I n_g . \quad (4)$$

While the other lines sought for high-temperature gas, Fe X λ6374 and Fe XIV λ5303, are not directly superimposed over single-absorption features, the continuum in these regions is complex enough on fine scales that a similar limit applies to their equivalent widths. This is shown in Figure 6, on a flattened spectrum of 3C 465 S.

The absolute calibration factors determined from standard star and photometric observations enter into the conversion from noise calculations in detected counts (eqs. [1]–[4]) and detectability limits on received flux. We require the flux received above the atmosphere, in units of energy per unit area, time, wavelength, and solid angle, corresponding to one detected photon per pixel. (The raw counts in ADUs are lower than the number of detected photons by a factor ~3). The standard-star calibrations give the needed conversion factors as a function of wavelength integrated over some spatial range (typically 6–10") chosen to encompass nearly all the scattered light, while the photometric calibration gives the required specific intensity conversion directly at the (single) effective wavelength of the R passband. We use these as zero points and use the standard-star data to determine the relative flux calibration of each galaxy spectrum as a function of wavelength.

Expressing the calibration factor for the system and a particular exposure time (for each line sought) as a pseudo-efficiency ϵ, we may write the specific intensity related to the detected counts n and exposure time t as

$$F = \frac{\epsilon n}{t \Delta\lambda \Omega} , \quad (\text{ergs cm}^{-2}\ \text{s sr}) \quad (5)$$

where $\Delta\lambda$ is the reciprocal dispersion in Å per pixel, and Ω is the solid angle subtended by each pixel (the angular scale along the slit times the projected slit width). The intensity of a line, integrated across I spectral channels and J spatial pixels containing n_l counts in the line, is then

$$F_{\text{line}} = \frac{\epsilon I n_l}{J \Delta\lambda t \Omega} . \quad (6)$$

That is, as expected, averaging decreases the detectable surface brightness. However, averaging over too large an area decreases the detectability of a discrete emission region through dilution. We therefore examine our limits point-by-point and consider averaged regions of various sizes in places of particular interest.

From these considerations, given the sky level and galaxy profile along the slit at any desired wavelength, we can construct a curve of the limiting detectable emission-line flux as a

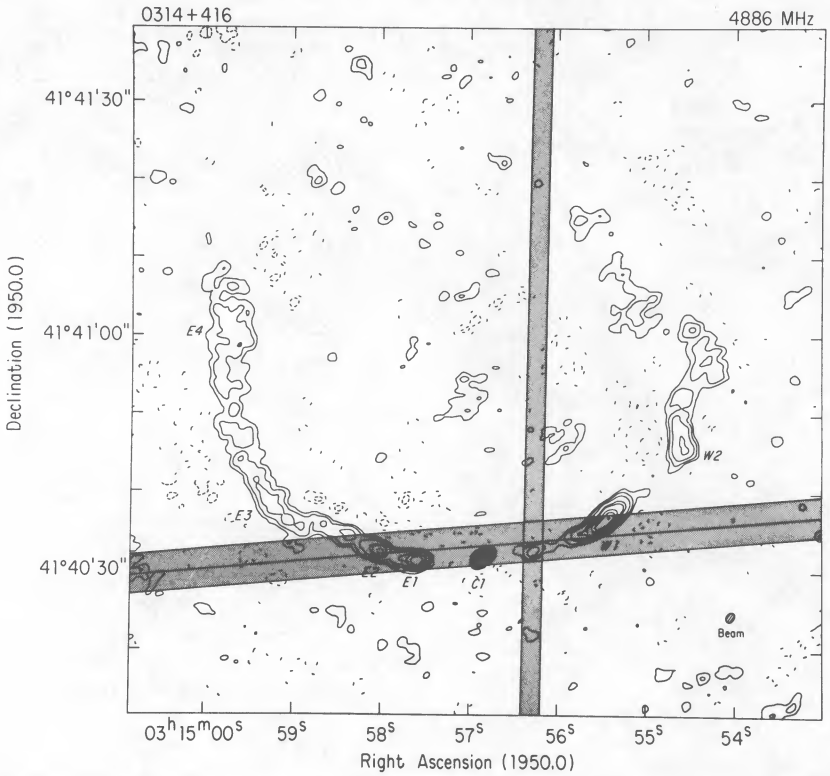

FIG. 4.—Contour plot of the radio source NGC 1265 showing the positions of the spectroscope slits (width 2".5 and width 5'). Contour plot is originally from Owen *et al.* 1978.

function of position along the slit. For convenience, we may represent the observed galaxy profile along each slit position by a nontruncated King function, relating the surface brightness σ at each position at distance r from the nucleus to that at the nucleus σ_0 according to

$$\sigma(r) = \frac{\sigma_0}{1 + (r/r_0)^2}, \tag{7}$$

where r_0 is the core radius of the fit. This core radius is a purely empirical quantity used to describe our data; it includes a strong contribution from seeing. As Schweizer (1979) has shown, seeing-convolved elliptical galaxy profiles of several kinds are very closely approximated by King functions in which r_0 has no physical significance. We thus caution against such interpretation of our values. This is particularly true for the spectra of NGC 1265 which do not pass through the galactic nucleus.

However, equation (7) is a good representation of the *observed* profiles of our objects, which is what is needed to estimate the quantities determining our detection limits. We list in Table 2 these parameters for each of our object spectra, with different exposures at the same position summed. From these values, the number of counts per pixel at any point may be closely approximated and a detection threshold calculated

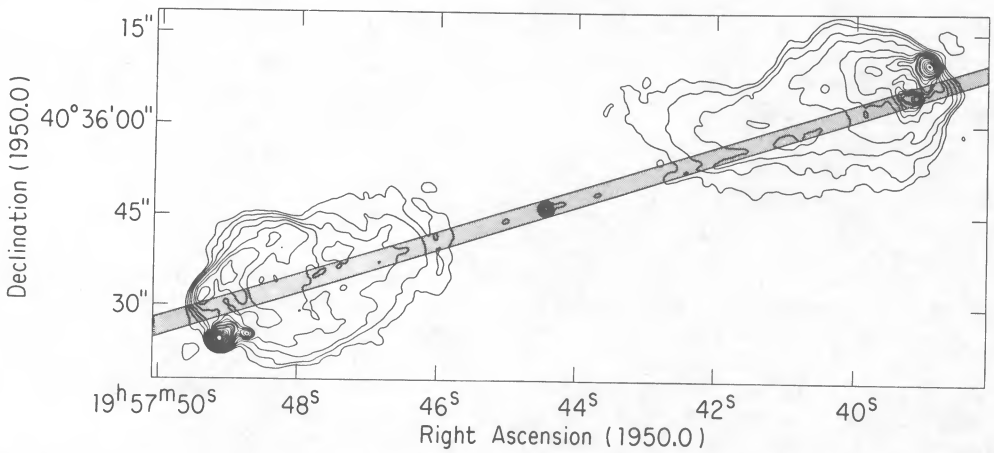

FIG. 5.—Contour plot of the radio source Cygnus A showing the positions of the spectroscope slits (width 2".5 and width 5'). Contour plot is originally from Dreher *et al.* 1987.

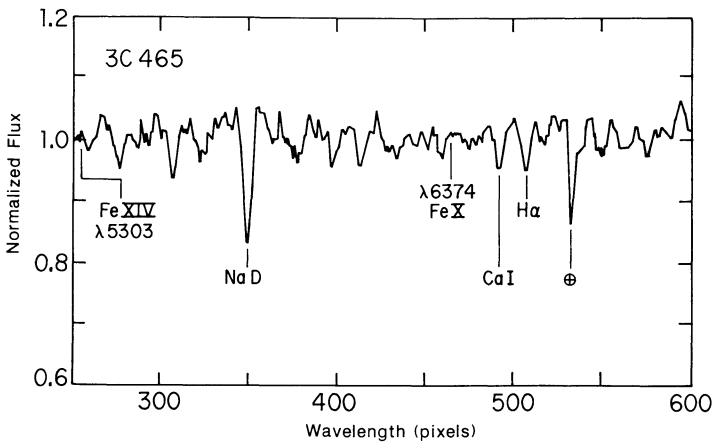

FIG. 6.—3C 465. One-dimensional spectrum of off-nucleus position showing the locations of the spectral lines of interest.

according to equations (1)–(4). The relevant quantities may be derived using

$$n_g = 3 \times n_0 \left[1 + \left(\frac{r}{r_0}\right)^2\right]^{-1} \quad (8)$$

in which the factor of 3 arises from the photon-to-ADU conversion; the number of sky photons detected is likewise $3n_s$. The readout noise is always 3 ADUs (9 photons) per exposure.

The spectra have been processed in several ways to search for any emission present above the thresholds just derived. Spatially unresolved or marginally resolved emission is seen in the nuclei of 3C 75 S, 3C 465, and (weakly) in NGC 1265. To see whether weaker extended emission is present, each spectrum was flattened in both dimensions through division by a smoothed version, which was created by convolving the original (flux-calibrated and sky-subtracted) spectrum with a box filter 100 Å long and one row high. This procedure preserves equivalent widths while removing the strong intensity gradients across the galaxies, so making changes in the strengths of absorption features or the shapes of small continuum regions apparent. As a check on results from inspection of these images, the median stellar continuum shape for each galaxy was subtracted from the images, allowing a straightforward determination of the statistical significance of any residuals.

These procedures showed no extended emission at Hα, Fe X, or Fe XIV in 3C 75 or 3C 465. Extended nuclear emission with strong velocity gradients appears in Hα and [N II] in 3C 31 (Fig. 10), while a very weak Hα feature *may* be present in NGC 1265. Flux limits at Hα are given in Table 3 for regions of particular interest. They are of order 10^{-18} ergs cm^{-2} s integrated across a typical expected cloud dimension. Limits for the Fe lines are essentially the same, within 30% in all cases; the strong temperature dependence of emissivity for these lines means that even an approximate flux limit translates into a distinct temperature limit.

c) *High-Dispersion Spectra of* 3C 31

To investigate the extended emission-line region found in 3C 31, a set of higher dispersion spectra was obtained, using a TI CCD at the Ritchey-Chrétien spectrograph of the KPNO 4 m telescope. The chip was binned 2 × 2 during readout to reduce the effects of the readout noise, giving a 400 × 400 image with pixels 0.″62 by 1.31 Å. The observed wavelength range was 6370–6893 Å, at a resolution set by the 1.″7 slit, of 3.0 Å FWHM. One hour exposures were obtained at position angles 162° and 72°, along and perpendicular to the inner part of the jet.

These spectra show extended line emission in both directions, approximately symmetric about the nucleus in both intensity and velocity structure. Velocity curves in Hα and [N II] λ6583 were measured using the curve-tracing routines in IRAF. The results are consistent with this emission originating in a rotating disk centered on the nucleus, whose orientation matches that of the dust lane or ring reported by Butcher, van Breugel, and Miley (1980). This model is described in § III*c*.

III. DISCUSSION

The upper limits to the flux of the Hα, Fe X, and Fe XIV lines can be used to obtain model-dependent constraints on the electron density (n_e) and the temperature (T) of the ionized gas. The (temperature dependent) emissivity (j) of these lines between temperatures of 10^4 and 4×10^6 is shown in Figure 7. The observed flux (F) from each line of a given ion with density n_i can be written

$$F = \frac{j n_e n_i V}{4\pi D^2}, \quad (9)$$

where V is the cloud volume (assuming a filling factor of unity), and D is the distance to the source. If the cloud can be characterized by some internal thermal pressure ($P = n_e kT$), where k is the Boltzmann constant, then equation (9) can be expressed as

$$F = \frac{j P^2 V_f}{4\pi k^2 T^2 D^2}, \quad (10)$$

where f is the fractional abundance of the relevant ion. For standard "solar" abundance we take $N_{Fe}/N_H = 4.0 \times 10^{-5}$

TABLE 2

GALAXY SPECTRUM PARAMETERS

OBJECT	P.A.°	COUNTS AT Hα		r_0		ϵ/t	POINT-SOURCE LIMIT
		Peak	Sky	Arcsec	Pixels	(ergs cm^{-2} s)	(ergs cm^{-2} s)
3C 465	145	4300	650	4.2	4.8	1.13×10^{-19}	3.3×10^{-18}
3C 465	136	1300	200	4.2	4.8	3.75×10^{-19}	6.0×10^{-18}
NGC 1265	95	3700	195	6.2:	7.2:	1.55×10^{-19}	2.5×10^{-18}
NGC 1265	95(N)	700	150	8.1	9.5	5.63×10^{-19}	7.9×10^{-18}
NGC 1265	178	420	260	9.5	11.0	1.18×10^{-18}	2.2×10^{-17}
3C 31	160	1900	200	2.8	3.3	1.38×10^{-18}	2.2×10^{-17}
3C 75 S	145	3000	500	3.8	4.4	1.93×10^{-19}	5.0×10^{-18}
Cygnus A	106	60	110	2.6	3.0	2.16×10^{-19}	4.1×10^{-18}

TABLE 3

Hα, Fe X AND Fe XIV LIMITS AT CLOUD AND JET POSITIONS

Object	Position	Offset (arcsec)	Flux Limit (ergs cm^{-2} s)	Flux arcsec^{-2}
3C 75 S	NW jet cloud	29–31 NW	1.7×10^{-17}	2.3×10^{-18}
3C 75 S	NW jet cloud	26–34 NW	3.7×10^{-17}	1.8×10^{-18}
3C 75 S	SE jet blob	26–34 SE	3.7×10^{-17}	1.8×10^{-18}
3C 75 S	SE jet blob	29–31 SE	1.7×10^{-17}	2.3×10^{-18}
3C 465	NW jet cloud	35–45 NW	3.0×10^{-17}	1.2×10^{-18}
3C 465	SE jet blob	40–56 SE	4.0×10^{-17}	1.0×10^{-18}
NGC 1265	W knot	5–7 W	4.0×10^{-17}	...
NGC 1265	W bend	13–15 W	3.0×10^{-17}	1.2×10^{-18}
NGC 1265	E knot	8–10 E	3.0×10^{-17}	...
3C 31	N jet	10–35 N	1.2×10^{-16}	1.9×10^{-18}
3C 31	S jet	10–35 S	1.6×10^{-16}	2.6×10^{-18}
Cygnus A	point in the radio lobes	>8 E or W	...	2.4×10^{-18}

NOTE.—NGC 1265 knots are treated as point sources and have no associated surface brightness. Also Cygnus A limits corrected for redding at Hα.

and $N_e/N_H = 1.18$ for fully ionized solar plasma (Allen 1973), giving $N_{Fe}/N_e = 3.4 \times 10^{-5}$. We assume solar abundance for 3C 465, 3C 75, 3C 31, and Cygnus A (see e.g., Pagel and Edmunds 1981). We take the abundance for NGC 1265 to be 0.5 solar as a plausible lower limit since the iron abundance in the ICM of the Perseus cluster is roughly one-half solar (Mushotzky and Smith 1980). Thus, even if the interstellar medium of NGC 1265 has been completely stripped and replaced by the intercluster medium (which is unlikely, see O'Dea and Owen 1987), the abundance should be at least roughly one-half solar.

For each radio source we will consider one or more volumes (see Table 3) in which the external pressure can be estimated. Plots of F versus T are shown in Figures 8, 9, 11, 12, and 13 for a region in each galaxy we have considered in detail. These results supercede the preliminary results of O'Dea, Owen, and Keel 1986 which contain a mistake in the interpretation of the surface brightness. Generally our results are weaker limits than O'Dea, Owen, and Keel 1986 but the qualitative conclusions of that paper remain generally valid. The input parameters to the curves are given in Table 4. The cloud sizes in the WATs are taken to be roughly the jet diameters near the bending area, since the clouds should be at least comparable to the jet sizes in order to deflect them. Previous observations of clouds or filaments of optical-line emission have shown typical projected sizes of 1–10 kpc in cluster cooling flows (e.g., Hu, Cowie, and Wang 1985) and associated with some radio galaxies (e.g., Baum *et al.* 1988).

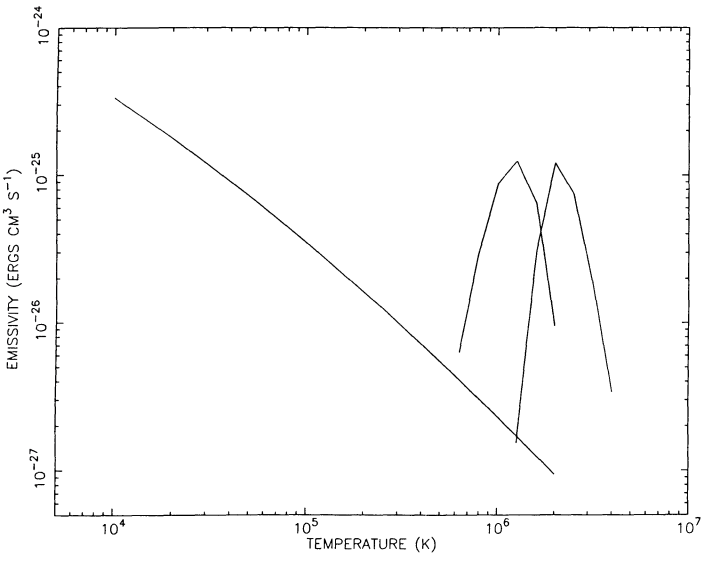

FIG. 7.—Emissivity vs. temperature for Hα (Ferland 1980), Fe X (λ6734), and Fe XIV (λ5303) (Nussbaumer and Osterbrock 1970). The Solar abundance of Fe has been assumed.

Most of our results are upper limits. However, we can use the knowledge of the external conditions, mainly from X-ray observations, pressure equilibrium, and equation (10) to constrain the conditions in and around the radio sources. From the combination of the three observed emission lines we have considered and the pressure balance assumption, generally a lower limit on T can be set. Then from the pressure balance assumption an upper limit on n can be obtained as well. The implications of these limits will be discussed for each source below.

In Figures 8, 9, 11, 12, and 13 the limits are displayed graphically for one example cloud size in each case. The reader can approximately evaluate other cloud sizes by shifting the surface brightness curves up or down by log V following equation (10). Since we have generally assumed cubical clouds, this means shifting by log $(r_{new}/r_{example})$.

a) 3C 465

Eilek *et al.* (1984) have discussed the problem of bending the jets of this radio galaxy. One mechanism is a collision with a

TABLE 4

INPUT PARAMETERS

Source	z	Cloud Radius (kpc)	Pressure[a] (10^{-12} dyn cm^{-2})	Metallicity[b]
3C 465	0.0322	2.5	3	1.0
3C 75	0.0232	2.5	4	1.0
NGC 1265	0.0183	0.5	20	0.5
3C 31	0.0167	2.5	10	1.0
Cygnus A	0.0566	0.5	40	1.0

[a] The external pressure is calculated from X-ray observations of the cluster gas: 3C 75 (Jones and Forman 1984), 3C 465 (Eilek *et al.* 1984), NGC 1265 (Fabian *et al.* 1981; Mushotzky and Smith 1980). For NGC 1265, $P = M^2 P_{ICM}$ where M ($\simeq 2$) is the galaxy Mach number through the ICM.

[b] Assumed fraction relative to solar abundance of Fe.

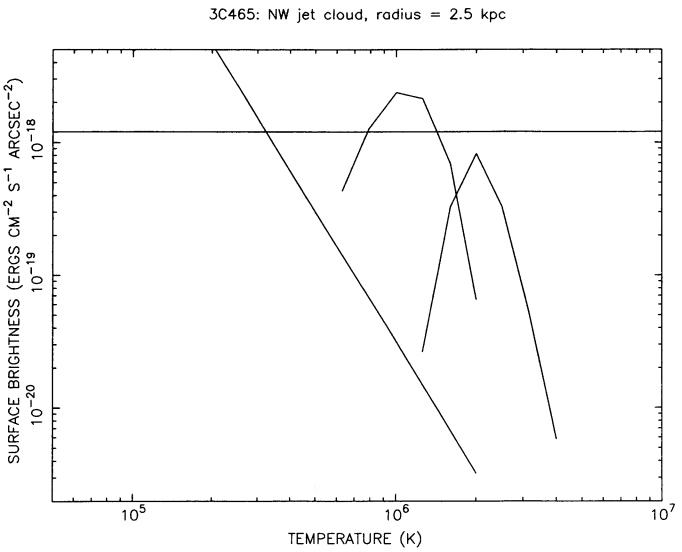

FIG. 8.—3C 465. Expected emission line flux as a function of temperature for the case of constant cloud pressure. Upper limits from these observations are shown for a region 40″ NW of the nucleus along the slit near the first bend in the northern jet. (See Fig. 1 and Table 2.)

cooler external cloud. Our observations of 3C 465 were designed to detect such clouds if they exist. From Eilek *et al.* the physical conditions in the external medium at 30″ from the nucleus (20 kpc) are $\sim T \sim 2 \times 10^7$ K and $n \sim 10^{-3}$ cm^{-3} based on *Einstein* IPC observations. Thus, $P_{\rm ext} \sim 3 \times 10^{-12}$ dynes cm^{-2}. If we used the models of Morganti *et al.* 1988, all the conclusions below would be stronger since they find a higher pressure for this cluster. We now will consider the possible existence of a cloud in pressure balance with this medium which would be capable of deflecting the jets.

If we first consider a cloud with a diameter equal to that of the jet ($r_{jk} \sim 1$ kpc) we can put an lower limit of 2.5×10^5 K on the temperature (shifting up Fig. 8 by log [2.5]). A larger cloud would have a higher temperature limit. Thus, we can rule out deflection by clouds at $\sim 10^4$ K which would be the expected temperature based on the cooling curve. Clouds at higher temperatures are harder to detect. How such a cloud would maintain a temperature above a few times 10^4 K is unclear but such a cloud would also be subject to evaporation in a hot ICM (Cowie and McKee 1977). From equation (24) of Eilek *et al.*, which describes cloud evaporation, and $P = nkT$, we can write

$$T \lesssim 5 \times 10^4 r_{ck} P_{-12} \tau_7^{-1} n_{-3}^{-1} , \quad (11)$$

where r_{ck} is the radius of the cloud in kpc, P_{-12} is the pressure in units of 10^{-12} dynes cm^{-2}, n_{-3} is the density of the ambient medium in units of 10^{-3} cm^{-3}, and τ_7 is the lifetime of the cloud in units of 10^7 yr. For $P_{-12} = 3$ and $n_{-3} = 1$,

$$T \lesssim 1.5 \times 10^5 r_{ck} \tau_7^{-1} . \quad (12)$$

This limit combined with the line-emission limit (eq. [10] and Fig. 8) requires $\tau_7 < 1$ for clouds with $r_{ck} < 2.5$ kpc. Clouds which are 10 kpc in radius would allow $\tau_7 \sim 2$, although it is not clear whether cool gas 20 kpc in diameter and only 20 kpc from the nucleus should be called a "cloud." Thus, the evaporation limit together with the emission line limits rule out the clouds unless we are in the situation that $T > 10^5$ K and $\tau_7 \lesssim 1$.

Assuming that the clouds must live for at least the lifetime of the observable source, $\tau_7 \lesssim 1$ implies an average velocity from the nucleus to the edge of the (~ 200 kpc) tails $\gtrsim 2 \times 10^4$ km s^{-1}. This would imply flow in the tails over most or all of their length which is very supersonic with respect to the external gas. Thus, we would expect to see evidence of shocks in the form of bright regions (or knots) as in many high-luminosity sources. Instead the tails look smooth, suggesting subsonic motion. Based on this argument we might expect τ_7 to be 20 or greater.

If the argument given above is wrong, $\tau_7 \sim 1$, and the jet is bent by an undetected cloud, then the flow velocity at the bend should be at least 20,000 km s^{-1}. Following Eilek *et al.* we impose the constraint that in order for the cloud to serve as an effective barrier it must not be accelerated to the velocity of the jet over the lifetime of the radio tails. Correcting a typographical error in their equation (21), we find that

$$n_j < 0.13 \left(\frac{r_{ck}^3 n_c}{v_3 r_{jk}^2 \tau_7} \right) , \quad (13)$$

where n_j is the density in the jet, n_c is the density in the deflecting cloud, r_{ck} is the radius of the cloud in kpc, and r_{jk} is the radius of the jet in kpc. Then, for $v_3 > 20$, n_j is less than $10^{-3}/\tau_7$ cm^{-3}. Thus, in this model, the density of the jet could be as large or larger than the background ICM density.

Thus, a model with deflecting clouds is possible but it requires cloud temperatures in the thermal unstable range (i.e., 10^5 to $\gtrsim 10^6$; Field, 1965), supersonic flow in the tails, and a corresponding source lifetime less than 10^7 yr. These parameters seem very unlikely but not possible to rule out absolutely.

b) 3C 75

The same general reasoning applies to 3C 75 as 3C 465, except that the pressure in the external medium near the bend in the southern-most jet based on the *Einstein* X-rays is $\sim P_{-12} = 4$ and $n_{-3} = 2$ (Jones and Forman 1984). Thus, the limit for a 2.5 kpc radius cloud is 3×10^5 K (Fig. 9) and for a 1 kpc cloud is $\sim 2.5 \times 10^5$ K. From equation (11), we get,

$$T \lesssim 4 \times 10^5 r_{ck} \tau_7^{-1} . \quad (14)$$

For a cloud with a radius of 1 kpc, $\tau_7 \gtrsim 0.6$; a cloud 2.5 kpc in radius requires $\tau_7 \gtrsim 4$. If from Figure 9, $T \gtrsim 3 \times 10^6$, then

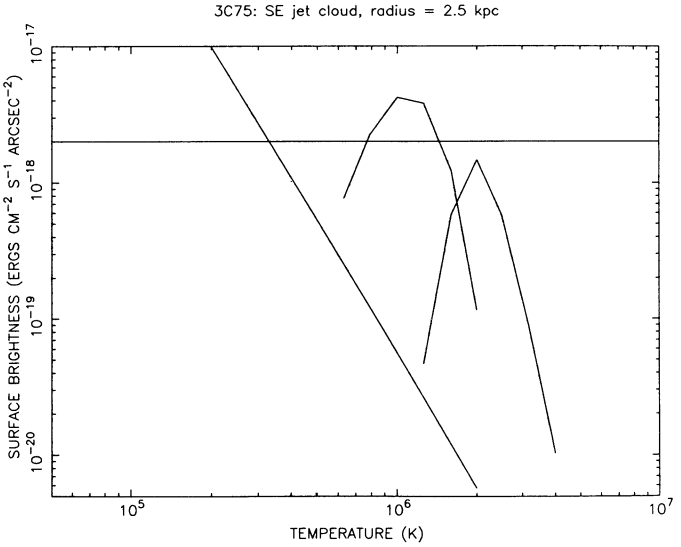

FIG. 9.—3C 75. Expected emission line flux as a function of temperature for the case of constant cloud pressure. Upper limits from these observations are shown for a region 30″ SE of the nucleus along the slit, near the bend in the southern jet. (See Fig. 2 and Table 2.)

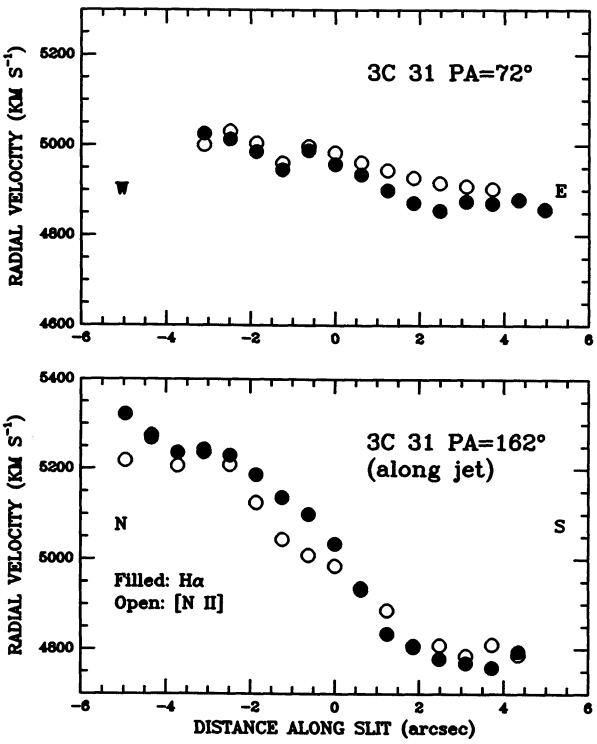

FIG. 10.—3C 31. Velocity curves for two slit positions.

$r_{ck} \gtrsim 30$ kpc which is greater than the distance of the cloud center to the nucleus of the galaxy and thus is not allowed. As for 3C 465, the velocity implied by the size of the source is at least 10^4 km s^{-1}, implying supersonic velocities relative to the external medium, while most of the outer source looks smooth suggesting subsonic velocities. As for 3C 465, a picture with hot ($>10^5$ K) clouds and large supersonic velocities in the outer parts of the source cannot be ruled out; but such a solution seems very unlikely.

c) 3C 31

As described in § IIc, spatially resolved emission lines were found around the nucleus of 3C 31. Most of the emission (in fact, all that was detected in the higher dispersion observations) is contained in a symmetric, roughly elliptical region about the nucleus (as well as can be judged from cuts in perpendicular positions). The velocity curves of this material (Fig. 10) show considerable symmetry, which motivated us to consider a rotating-disk model.

A simple solid-body disk was modeled, since the inner parts of the velocity curves are nearly linear (for radii less than 2″ in position angle 162°, for example). The inclination and line of nodes of such a disk may be obtained from the ratio of central velocity gradients in two position angles. In this case, the slit positions do not coincide with the projected kinematic axes of the disk, so an ambiguity in position angle exists. Formally, the major axis lies 23° from the jet axis, at PA 139° or 5° (formal error ±4°); the former value agrees closely with the dust-lane orientation, and we consider it correspondingly more likely. The disk inclination is not well determined, but lies 25°–40° from the line of sight, based on the turnover points in the velocity curves. The observed emission extends outward from the nucleus approximately to the position of the dust ring.

Properties of the gaseous disk are:

(1) Central radial velocity $v_{obs} = 5060 \pm 30$ km s^{-1} (heliocentric). (2) Maximum rotation velocity ± 300 km s^{-1} at a distance 3.″6 or 1.2 kpc. (3) The inner edge of the dust lane is 3.″5 from the nucleus at PA 135. The emission in the disk is similar in line ratios to that at the nucleus, with [N II] λ6583/Hα = 1.5, and [S II] λλ6717, 6731/Hα = 0.5 and [O III] λ5007/Hα ∼ 0.1. These are not characteristic of photoionization by OB stars (Baldwin *et al.* 1980), so the disk ionization is likely driven by the nucleus. The mechanism for this is less clear, since energy supply by kinetic means (shocks) and photoionization from a weak, flat-spectrum source produce almost identical emission-line spectra in the optical (e.g. Keel 1985). A weak broad component is probably present at a low level. The disk is of relatively high density ($n_e \sim 300$ cm^{-3}), from the [S II] doublet ratio. In a photoionization model, the ionization parameter needed to account for the observed line ratios requires an isotropic luminosity in the Lyman continuum of order 7×10^{52} photons s^{-1} or 5×10^{42} ergs s^{-1} for a source with a power-law spectral index of −1, from 1–4 rydbergs. The associated optical continuum would be too weak to detect with the current data, against the starlight background of the galaxy.

No line emision was detected from the outer jet. Morganti *et al.* (1988) have modeled the *Einstein* X-ray data and find a pressure of $\sim 1.3 \times 10^{-11}$ dynes cm^{-2} which is similar to conditions in the centers of rich clusters. Using this model and our limit in Table 2, $T > 3 \times 10^6$ K and $n_j < 0.03$ cm s^{-3} at this point (see Fig. 11). These limits appear to rule out the heavy jet model of Blandford and Icke (1977) and thus add strength to the more recent light jet models (e.g., Bicknell 1986).

d) NGC 1265

No extra-nuclear emission was detected in any of the regions searched in NGC 1265. We can use these limits to place constraints on the temperature and density of thermal gas in (1) the ISM of NGC 1265, (2) the inner knots of the radio jets, and (3) clouds formed by thermal instabilities in a possible galactic bow shock or galactic wake.

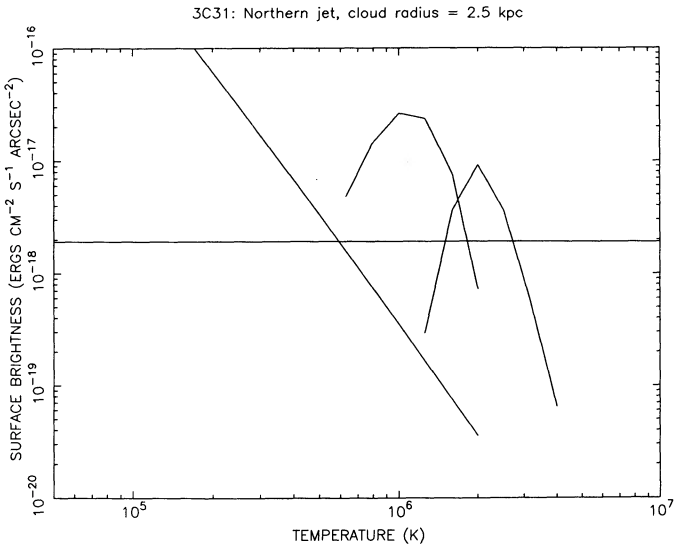

FIG. 11.—3C 31. Expected emission line flux as a function of temperature for the case of a constant jet pressure. Upper limits from these observations are shown for a region 10 to 35 arcsec north of the nucleus along the slit. (See Fig. 3 and Table 2.)

1. O'Dea and Owen (1986, 1987) have noted that the existence of the steep spectrum cocoon around the radio jets, the Rotation Measure gradients, and the total intensity and collimation structure of the jets provide strong evidence for an ISM in NGC 1265. Thus, we consider the constraints that these spectroscopic observations place on the ISM.

The pressure in the ISM of NGC 1265 has not been directly measured, however, there are two ways to estimate it. The minimum radio pressure in the radio jets is $\sim 2 \times 10^{-11}$ dynes cm^{-2} (O'Dea and Owen 1986, 1987). We can assign this pressure to the ISM assuming that the jets are near minimum pressure conditions and that the jets are also confined by thermal pressure from the ISM. Alternately, for transonic galaxy motion through the ICM with Mach number M_g, the ISM pressure is $P_{\rm ISM} \simeq M_g^2 P_{\rm ICM}$. Then, taking a galaxy velocity of $v_g \geq 2200$ km s^{-1} (Chincarini and Rood 1971), ICM sound speed of ~ 1000 km s^{-1} (for $T = 7 \times 10^7$ K, Mushotzky and Smith 1980) and particle density of $n_{\rm ICM} = 5 \times 10^{-4}$ cm^{-3} (Fabian *et al.* 1981) gives $P_{\rm ISM} \geq 2.4 \times 10^{-11}$ dynes cm^{-2} which is similar to the previous estimate. We adopt a value of $P_{\rm ISM} = 2 \times 10^{-11}$ dynes cm^{-2} for the analysis which follows.

We consider an emitting volume in the ISM which consists of a cylinder with a depth of 15 kpc and a projected area equal to that of our slit area at the positions considered in Table 3. We obtain a lower limit to the temperature of $T > 3 \times 10^6$ K and a upper limit to the density of $n < 5 \times 10^{-2}$ cm^{-3} (see Fig. 12). These limits are roughly consistent with the values estimated by Jones and Owen (1979) assuming a balance between ram pressure stripping and stellar mass loss (see also Lea and De Young 1976). The limit of $T > 3 \times 10^6$ K is lower than the typical temperature of $T \sim 10^7$ K found for the X-ray coronae in isolated ellipticals (Forman, Jones, and Tucker 1985).

Rotation Measure (RM) variations along the radio jets of ~ 30 rad m^{-2} were found by (O'Dea and Owen 1986). These changes are too large to be produced inside the jets (see O'Dea and Owen 1986 and must be produced in an external screen in front of the jets (most likely the ISM). The RM is given by RM $= 800 n B_l L$ rad m^{-2} where n is the electron density in cm^{-3}, B_l is the net line-of-sight component of the magnetic field in 10^{-6} Gauss (μG), and L is the path length through the ISM in kpc. Taking $L = 10$ kpc and $n < 5 \times 10^{-2}$, gives an upper limit of $B_l > 0.08$ μG.

2. Assuming the same value for the pressure, we can also obtain lower limits to the temperature of the gas in the inner knots in the radio jets (E1, E2, W1, W2-W3, see Fig. 3 and O'Dea and Owen 1986) of $T > 1$–3×10^5 K (Fig. 12). These limits are weaker than for the ISM because of the smaller emitting volumes considered. The limits to the temperature correspond to upper limits to the density of $n < 0.5$–1.5 cm^{-3}.

These results imply that the mass flux of the radio jets is not dominated by *cold* ($T \sim 10^4$ K) gas in pressure balance with the radio-luminous plasma. One possibility is that the pressure of the thermal gas may be much less than that of the radio-luminous plasma. The lack of a significant contribution to the pressure from the thermal gas would be consistent with the general agreement of the estimated minimum radio pressure (in diffuse regions of edge-darkened radio jets) with the external pressure. In addition, the thermal particle density in the jets could be quite low. Using constraints on energy and momentum flux in the jets in NATs, O'Dea (1985) estimated densities of $\sim 10^{-4}$–10^{-6} cm^{-3} for the quasi-continuous beam models (Begelman, Rees, and Blandford 1979; Jones and Owen 1979) and ~ 1–0.01 cm^{-3} for the multiple plasmon in a channel model (Christiansen, Pacholczyk, and Scott 1981). The limits derived here are clearly consistent with the beam models and only marginally consistent with the multiple plasmon model.

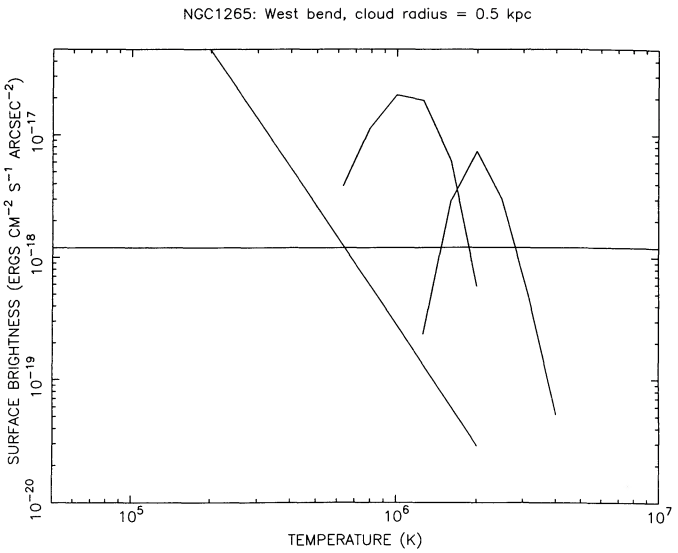

FIG. 12.—NGC 1265. Expected emission line flux as a function of temperature for the case of constant cloud pressure. Upper limits from these observations are shown for a region 14″ west of the nucleus near the bend in the jet. (See Fig. 4 and Table 2.)

3. We also failed to detect any emission from clouds which might have formed from thermal instabilities in the galactic bow shock or wake of NGC 1265. For a 1 kpc diameter cloud, the lower limit to the temperature is $T > 1.5 \times 10^6$ K, and the upper limit to the density is $n < 0.1$ cm^{-3} assuming these clouds would have pressures similar to that of the ISM. Lower pressures would make these clouds harder to detect. Possibly, heating of the gas compensates for any enhanced cooling that might occur due to compression of the gas at these locations. We should point out that the formation of such clouds is not required by the existence of bow shocks or wakes.

e) Cygnus A

The external pressure from the X-ray emitting gas around Cygnus A is very high, $nT \sim 4 \times 10^6$ cm^{-3} K. Even higher pressures might occur through interactions with the radio lobe. However, no line emission was detected more than a few arcsec from the nucleus. Our upper limit to the emission line flux from region of the lobes (and any point away from a star $>8''$ from the nucleus) is 10^{-16} ergs cm^{-2} s^{-1} (corrected for reddening).

As noted earlier Dreher, Carilli, and Perley (1987) report very large rotation measure gradients across the lobes of Cygnus A. The large observed values which rotate the $\boldsymbol{E}$ vectors through many radians can only be caused by a foreground screen not by thermal plasma mixed with the radio emitting particles. This leads Dreher, Carilli, and Perley (1987) to discuss both the general cluster medium and a hypothetical sheath surrounding the radio lobes. Models of the plasma producing the X-ray emission detected by *Einstein Observatory* suggest an a very hot medium near the lobes with a temperature, $T \sim 7 \times 10^7$ K, and a density, $n \sim 6 \times 10^{-3}$ cm^{-3}. (Arnaud *et al.* 1984). A sheath around the lobes thus would likely have a pressure of at least $nT \sim 4 \times 10^5$ cm^{-3} K. If the sheath was behind part of a shocked layer, it might have a higher pressure, possibly $nT \sim 5 \times 10^6$ cm^{-3} K and a thickness of ~ 1 kpc (Norman *et al.* 1982; Williams and Gull 1984).

Other scenarios might be envisioned; however, the point of

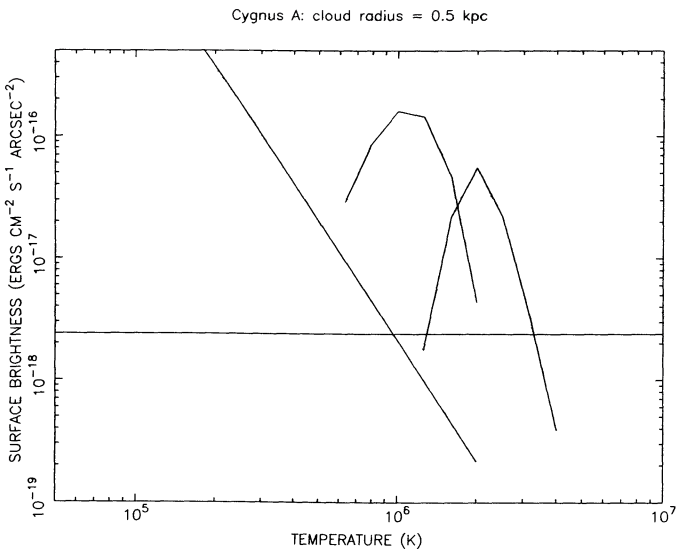

FIG. 13.—Cygnus A. Expected emission line flux as a function of temperature for the case of constant cloud pressure. Upper limits from these observations are shown for any 0.5 kpc region more than 8″ from the nucleus along the jet. (See Fig. 5 and Table 2.)

our observations is that the screen doing the rotation is probably made up of hot gas since we see no line emission. For example, Figure 13 shows expected emission line flux from a region 1 kpc in thickness with a pressure of 5×10^5 cm^{-3} K. We should see emission from such a region if $T < 2.5 \times 10^6$ K. For a lower temperature, e.g., $T \sim 10^4$ K, the thickness of a sheath would need to be less than 0.1 pc to avoid detection. For a screen with 0.1 pc thickness and $nT \sim 4 \times 10^5$ cm^{-3} K, $n \sim 50$ cm^{-3}. To produce a characteristic Faraday rotation of 2000 radians m^{-2}, we require a line of sight magnetic field of $B_{\parallel} \sim 500$ μG. However, such a B field would exert a pressure of $nT \gtrsim 8 \times 10^7$ cm^{-3} K and would appear to contradict the X-ray observations. Other combinations of parameters for $nT > 4 \times 10^5$ and $T < 4 \times 10^5$ K appear to produce contradictions. Thus we conclude that the medium producing the roation is at a high temperature, $>2 \times 10^6$ K and probably at the temperature of the X-ray emitting gas.

Pierce and Stockton (1986) have noted strongly different distributions of Hα and continuum radiation in Cygnus A. Our slit position is close to the direction of greatest separation as shown on their images, so we have examined our data for any further information on the distribution of emission from various lines. All the lines we measured (i.e., Hα + [N II], [O III], [O I], [S II], [N I], and [Fe X]) are centered at the same location, in agreement with their results. This point is 0.9 ± 0.1 west of the continuum centroid at Hα, which moves eastward with decreasing wavelength. With our modest spatial resolution (~2″.5 FWHM), we can conclude that the lines all appear to have nearly the same extent.

V. CONCLUSIONS

Although we detected extra-nuclear emission in only one of the five cases, we can make interesting deductions about proposed models in each case.

1. Models using cool deflecting clouds for bending 3C 465 and 3C 75 seem unlikely, although models with both hot clouds and high velocities for both sources cannot be ruled out.

2. A rotating gaseous disk, first reported by Butcher, van Breugel, and Miley (1980), can be seen in emission-line gas in the center of 3C 31. The model with heavy jets bent by gravitational deflections for 3C 31 (Blandford and Icke 1977) appears to be ruled out.

3. The temperature in the interstellar medium in NGC 1265 appears to be above 3×10^6 K. This suggests that the interstellar magnetic field necessary to explain the observed Faraday rotation gradients is greater than 0.08 μG.

4. The large rotation measures seen in the lobes of Cygnus A are likely to be produced by a foreground screen of *hot* gas $>10^6$ K.

REFERENCES

Allen, C. W. 1973, *Astrophysical Quantities* (London: University Press).
Arnaud, K. A., Fabian, A. C., Eales, S. A., Jones, C. and Forman, W. 1984, *M.N.R.A.S.*, **211**, 981.
Baldwin, J. A., Carswell, E. J., Wampler, E. J., Smith, H. E., Burbidge, E. M., and Boksenberg, A. 1980, *Ap. J.*, **236**, 388.
Baum, S., Heckman, T., Bridle, A., van Breugel, W., and Miley, G. 1988, *Ap. J. Suppl.*, **68**, 643.
Begelman, M. C., Rees, M. J., and Blandford, R. D. 1979, *Nature*, **279**, 770.
Bicknell, G. 1986, *Ap. J.*, **300**, 591.
Blandford, R. D., and Icke, V. 1977, *M.N.R.A.S.*, **181**, 559.
Butcher, H. R., van Breugel, W., and Miley, G. K. 1980, *Ap. J.*, **235**, 749.
Chincarini, G., and Rood, H. J. 1971, *Ap. J.*, **168**, 321.
Christiansen, W. A., Pacholczyk, A. G., and Scott, J. S. 1981, *Ap. J.*, **251**, 518.
Cowie, L. L., and McKee, C. F., 1977, *Ap. J.*, **215**, 135.
De Young, D. S. 1986, *Ap. J.*, **254**, 62.
Dreher, J. W., Carilli, C. L., and Perley, R. A., 1987, *Ap. J.*, **316**, 611.
Eilek, J. A., Burns, J. O., O'Dea, C. P., and Owen, F. N. 1984, *Ap. J.*, **278**, 37.
Fabian, A. C., Hu, E. M., Cowie, L. L., and Grindlay, J. 1981, *Ap. J.*, **249**, 47.
Ferland, G. 1980, *Pub. A.S.P.*, **92**, 596.
Field, G. B. 1965, *Ap. J.*, **142**, 531.
Fomalont, E. B., Bridle, A. H., Willis, A. G., and Perley, R. A. 1980, *Ap. J.*, **237**, 418.
Ford, H. C., and Butcher, H. 1979, *Ap. J. Suppl.*, **74**, 116.
Forman, W., Jones, C., and Tucker, W. 1985, *Ap. J.*, **293**, 102.
Heckman, T. M., van Breugel, W. J. M., and Miley, G. K. 1984, *Ap. J.*, **286**, 509.
Hu, E. M., Cowie, L. L., and Wang, Z. 1985, *Ap. J. Suppl.*, **59**, 447.
Jones, C., and Forman, W. 1984, *Ap. J.*, **276**, 38.
Jones, T. W., and Owen, F. N. 1979, *Ap. J.*, **234**, 818.
Lea, S. M., and De Young, D. S. 1976, *Ap. J.*, **210**, 647.
Keel, W. C. 1983, *Ap. J.*, **269**, 466.
———. 1985 in *Astrophysics of Active Galaxies and Quasars*, ed. J. S. Miller (Mill Valley, CA: University Science Books), p. 1.
Morganti, R., Fanti, R., Gioia, I. M., Harris, D. E., Parma, P., and de Ruiter, H. 1988, *Astr. Ap.*, **189**, 11.
Mushotzky, R., and Smith, B. 1980, *Highlights Astr.*, **5**, 735.
Norman, M. L., Smarr, L., Winkler, K.-H. A., and Smith, M. D. 1982, *Astr. Ap.*, **113**, 285.
Nussbaumer, H., and Osterbrock, D. E. 1970, *Ap. J.*, **161**, 811.
O'Dea, C. P. 1985, *Ap. J.*, **295**, 80.
O'Dea, C. P., and Owen, F. N. 1986, *Ap. J.*, **301**, 841.
———. 1987, *Ap. J.*, **316**, 95.
O'Dea, C. P., Owen, F. N., and Keel, W. C. 1986, *Canadian J. Phys.*, **64**, 369.
Owen, F. N., Burns, J. O., and Rudnick, L. 1978, *Ap. J. (Letters)*, **226**, L119.
Owen, F. N., O'Dea, C. P., Inoue, M., and Eilek, J. A. 1985, *Ap. J. (Letters)*, **294**, L85.
Owen, F. N., and White, R. A. 1990, in preparation.
Pagel, B. E. J., and Edmunds, M. G. 1981, *Ann. Rev. Astr. Ap.*, **19**, 77.
Pierce, M. J., and Stockton, A. 1986, *Ap. J.*, **305**, 204.
Pritchet, C. 1977, *Ap. J. Suppl.*, **35**, 397.
Schweizer, F. 1979, *Ap. J.*, **233**, 23.
Williams, A. G., and Gull, S. F. 1984, *Nature*, **310**, 33.

WILLIAM C. KEEL: Department of Physics and Astronomy, University of Alabama, P.O. Box 870234, Tuscaloosa, AL 35487

CHRISTOPHER P. O'DEA: Postbus 2, Radiosterrenwacht Dwingloo, 7990 AA Dwingeloo, Netherlands, 05219-7244

FRAZER N. OWEN: NRAO, P.O. Box O, Socorro, NM 87801